Bit Error Rate Measurements in Reverberation Chambers Using Real-Time Vector Receivers

S. J. Floris, K. A. Remley, *Senior Member, IEEE*, and C. L. Holloway, *Fellow, IEEE*

***Abstract*—We discuss practical measurement implementation methods when using laboratory-grade vector instrumentation to measure bit error rate (BER) in the highly reflective, time-variant environment of a reverberation chamber. These methods include synchronizing the transmitted and received signals in spite of time-varying path lengths created in the reverberation chamber and minimizing potential receiver loss of lock after a long-duration fade by use of a simple error-correction scheme. Use of general laboratory instrumentation, rather than application-specific digital receivers, facilitates study of the multipath channel created in the reverberation chamber on BER.**

***Index Terms*—Bit error rate (BER), digital modulation, reverberation chamber, vector signal analyzer (VSA), vector signal generator (VSG), wireless communications.**

I. Introduction

In RECENT years, the use of reverberation chambers as a reliable, repeatable, and controllable environment has become increasingly popular for testing wireless devices and systems. These applications include: measurement of K factor [1], measurement of radiated power from mobile phones [2], measurements on multiple-input–multiple-output (MIMO) systems [3], simulated channel testing in Rayleigh multipath environments [4]–[6], and measurements of receiver sensitivity of mobile terminals [7].

Most prior work in the area of wireless has focused on characterization of the reverberation chamber using a vector network analyzer (VNA) to conduct stepped-frequency measurements (for example, [1] and [4]–[6]) or on application-specific uses of the reverberation chamber where specialized receivers were used (for example, [2], [3], and [7]). However, to study the effects of the physical propagation channel created by the reverberation chamber on a digitally modulated signal, it is desirable to use laboratory-grade, real-time instrumentation such as vector signal analyzers (VSAs), real-time spectrum analyzers, and real-time oscilloscopes. Digital receivers used for specific applications incorporate manufacturer-specific demodulation, error correction, and equalization techniques designed to minimize bit errors. In the present case, it is our goal to study—not suppress—bit errors. Thus, we discuss measurement issues related to the use of vector real-time receivers for measurement of the effects of the highly reflective, time-variant channel created by the reverberation chamber on bit error rate (BER). These measurement issues include accomplishing synchronization between the transmitter and receiver in the presence of time-varying path delays and loss of lock by the receiver after deep fades when a digitally modulated signal having no built-in error correction is measured. We describe straightforward methods of overcoming these issues when using commercially available test equipment such as a vector signal generator (VSG) and a VSA. This enables the study of reverberation-chamber-induced effects rather than receiver-induced or application-specific effects on BER.

Manuscript received April 08, 2010; revised June 03, 2010; accepted June 09, 2010. Date of publication June 21, 2010; date of current version July 12, 2010.

S. J. Floris is with the National Institute of Standards and Technology (NIST), Boulder, CO 80305 USA, and also with the Faculty of Electrical Engineering, Eindhoven University of Technology, 5600 MB Eindhoven, The Netherlands.

K. A. Remley and C. L. Holloway are with the National Institute of Standards and Technology (NIST), Boulder, CO 80305 USA (e-mail: remley@boulder.nist.gov).

Color versions of one or more of the figures in this letter are available online at http://ieeexplore.ieee.org.

Digital Object Identifier 10.1109/LAWP.2010.2053513

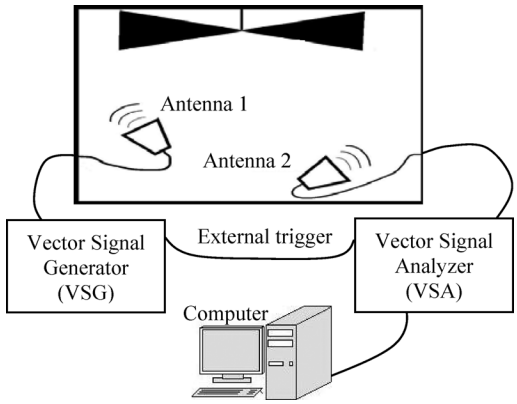

Fig. 1. Schematic overview of the measurement setup.

II. Measurement Setup

An overview of the measurement setup is shown in Fig. 1. The unloaded reverberation chamber used in our tests is $2.8 \times 3.1 \times 4.6$ m^3 in size and is located at the National Institute of Standards and Technology (NIST), Boulder, CO. The VSG and the VSA were connected to low-frequency dual-ridge horn antennas. These antennas have a range of 200 MHz–2 GHz and dimensions $0.93 \times 0.98 \times 0.73$ m^3. We verified that the near-field coupling of the electrically large antennas did not significantly affect our measurements by noting that a single-frequency measurement of received power showed deep fades down to -55 dB when the paddle was rotating. Near-field effects would reduce the depth of these fades.

We generated a digitally modulated signal with the VSG. The VSA was then used to demodulate the received frames from the chamber as well as to measure the average power in each frame. The system was calibrated by directly connecting the VSA and VSG together to ensure the digitally modulated signal was received error-free. When the instruments were then connected to the antennas, errors were presumed to arise from the multipath channel created in the reverberation chamber. The BER

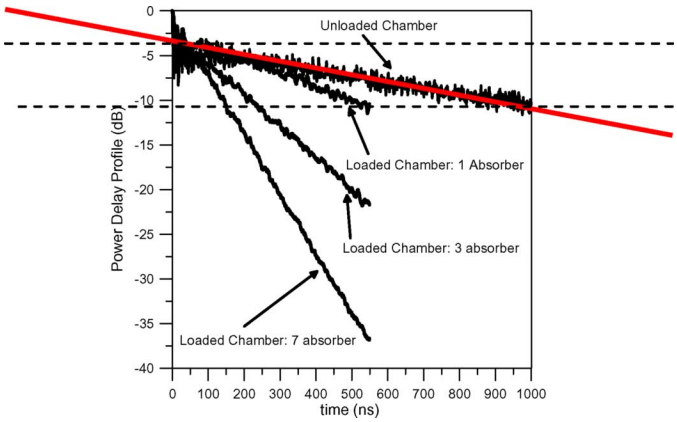

Fig. 2. Power-delay profile measured in the NIST reverberation chamber.

was calculated by the ratio of erroneously received bits to the total number of received bits. The movement of the paddle was controlled by the computer.

III. Signal Construction

To focus our study on the measurement of impairments to the propagation channel created in the reverberation chamber, we generated a binary phase-shifted keyed (BPSK) digitally modulated signal not tied to any specific wireless standard or error-correcting algorithm. A frame of 2048 pseudorandom bits was generated by the Marsenne Twister algorithm [8]. This algorithm is designed to achieve a statistically uncorrelated sequence that has a white-noise-like autocorrelation. This single 2048-bit frame was BPSK-modulated by the VSG and transmitted repeatedly into the reverberation chamber. One 2048-bit pattern was used for simplicity. By observing the symmetry of the autocorrelation function, we concluded that the results were not skewed by our choice of frame. The frame length was chosen such that the power of the first bit in the frame had decayed significantly before the next frame was transmitted to ensure that correlation between successive frames in the multipath environment was minimized.

The decay period of a short pulse can be found from the power-delay profile (PDP) of the unloaded reverberation chamber, which can be measured with a VNA, as discussed in [9], [10]. For the unloaded reverberation chamber, extrapolation of the PDP in Fig. 2 shows a vertical slope of approximately -7 dB/μs. In our BER measurements, the highest symbol rate we used was 768 000 symbols per second (sps), corresponding to a frame rate of 2.7 ms. This means that the signal decays faster than the shortest frame rate used in the measurements, such that the pseudorandom nature of the signal is maintained.

IV. Using the VSA as a Receiver

The VSA has been designed to make vector measurements such that both amplitude and phase information of the received signal are available [11]. Use of the phase information enables demodulation of a digitally modulated signal. We set the digital demodulator in the VSA to demodulate the 2048-bit frame of the received signal.

We used the trigger-delay setting in the VSA to correct for the average path delay between the VSG and the VSA. However, the reverberation chamber produces a time-varying multipath environment, resulting in a time-varying delay between the arrival of a trigger pulse and the arrival of the first bit of each frame. If this delay exceeds a 1-bit duration, an overall offset is introduced, which results in an incorrect comparison and therefore an incorrect BER calculation. This offset was found and corrected with the aid of a cross correlation of the known bits and the received bits. An indication of the severity of this delay is as follows: When using a BPSK signal with a symbol rate of 768 ksps, we observed a maximum deviation in offset of 3 bits. If this time-varying offset were not corrected, the BER we calculate would be artificially high.

The VSA uses the fast Fourier transformation (FFT) to find the frequency components of the digitized signal, which is the most time-consuming operation of each measurement iteration [11]. The processing time easily exceeds the transmission time of each frame, so not all frames were measurable in real time. For stepped-paddle measurements, we added a delay between each measurement.

However, when continuous-paddle measurements were performed, all sequential frames needed to be collected as soon as the paddle started rotating so that we could study the effects of fading. The recording feature of the VSA was used to overcome the inability of the VSA to process all frames sequentially in real time. The digitized signal was stored in memory until the raw data collection was completed. The analyzer then stepped through the recording in offline post-processing. A disadvantage of using a recording is that the external trigger pulses are not marked. Although the recording was started at the arrival of the external trigger signal, the synchronization of all successive frames then relied on the stability of the VSG.

V. Error-Correcting Algorithm

As mentioned, in our one-way communication system, no standardized, real-time error-detecting or error-correcting algorithm was used. Bit errors found by data comparison at the receiving end of the setup were either caused by the time-varying multipath environment (which we wish to study) or by the receiving instrumentation (which we do not). For example, consider the environment to be such that the receiver measures a faded signal. If an odd number of phase transitions of the BPSK-signal remain undetected, a redetermination of the phase at the start of a frame leads to an incorrect (inverted) symbol definition and thus a stream of errors. In wireless communications, this loss of symbol definition is known as a burst error, which is generally corrected using resynchronization information embedded in the transmitted data. The data we transmit has no such information. Thus, while a deep fade caused the burst error to occur in the example, the burst duration is not directly related to the physical source of the fade. In essence, the receiver artificially increases the burst duration. The main challenge now is to discriminate between the bit errors introduced by the channel and bit errors introduced by the receiver.

To study the causes of bit errors due to the channel impairments presented by the reverberation chamber, errors due to loss of the symbol definition during a long fade were reduced by our use of a simple error-correcting algorithm in post-processing. In wireless applications, data are typically transmitted in packets. An error-detecting and/or error-correcting protocol usually is in place, such that an entirely inverted packet either can be corrected or neglected and retransmitted in the worst case.

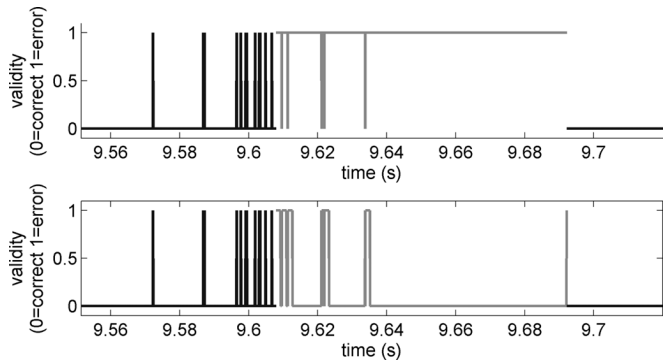

Fig. 3. Error-correcting algorithm applied to several short-duration burst errors and one long burst error.

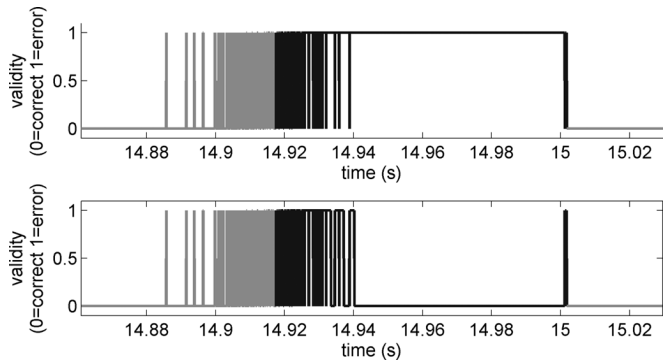

Fig. 4. Error-correcting algorithm applied to a heavily distorted frame.

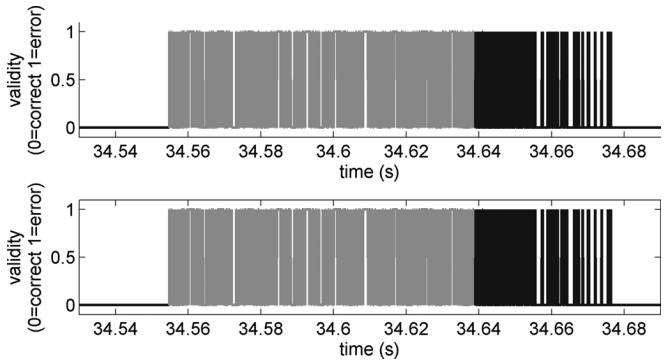

Fig. 5. Error-correcting algorithm does not influence a severely distorted bit-error sequence caused by the multipath channel.

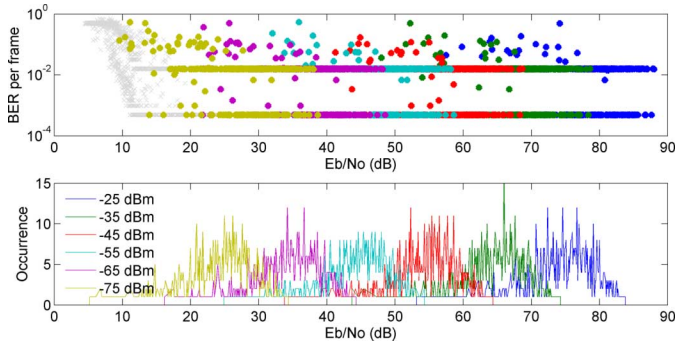

Fig. 6. BER per measured frame for a 24.3-ksps BPSK signal and a 2-rpm continuously moving paddle. The legend lists the transmit powers applied in the six different measurements.

To simulate such behavior, we considered our 2048-bit frame as containing multiple 32-bit packets. Any loss of symbol definition longer than 32 bits was considered a burst error. These were corrected in post-processing, such that the algorithm left only 32 erroneous bits, simulating one lost packet. This simple scheme has the advantage that bit errors due to limitations of the instrumentation's ability to decode the signal do not dominate the BER calculation. The algorithm does not correct the last bit error of the original burst error to mark the position where the error correction stopped.

To illustrate this error-correcting scheme, consider a measured bit-error pattern as shown in the top graph of Fig. 3, which shows several short-duration burst errors and one long-duration burst error in the light-gray-colored frame starting at around 9.61 s. The frame started off with an error (shown by a "1"), and the majority of the frame appeared to contain bit errors. At approximately 9.69 s, the dark-gray-colored frame again produced correct results (shown by a "0"), indicating that the inverted light-gray-colored frame suffered from lost synchronization. The lower graph shows the behavior when the error-correcting algorithm was applied. We applied the error correction scheme to the burst errors so that these long burst errors did not dominate the BER results. Note that the transition at the end of the light-gray-colored frame (at approximately 9.69 s) is also marked as an error.

More severe bit error patterns are shown in Fig. 4. The light-gray-colored frame does not indicate a long-duration burst error, as evidenced by the rapid transient bit errors, so these errors were likely caused by the time-varying multipath environment. The lower graph shows that these errors of interest are not affected by the error-correcting algorithm, but the burst error in the dark-gray-colored frame was replaced by short 32-bit error packets.

A severely distorted frame is shown in Fig. 5. The lower graph shows that errors persist even though error correction was applied. This indicates that bit errors caused by impairments of the channel have occurred and been measured properly. This effect is of special interest in this study. Note that we ensured that the error-correcting algorithm did not introduce bit errors in an unimpaired channel.

VI. BER Results

We measured BER for a 24.3-ksps BPSK signal with both a stepped paddle and a continuously moving paddle. In this section, we present representative results to examine the effects of the error-correcting algorithm on the overall BER value. Details shown in the figures will be discussed in a future publication.

The BER per measured frame was calculated and is shown for six different transmit powers in the top graph of Fig. 6 for a 2-rpm continuously moving paddle. Every highlighted dot in the graph represents a BER calculation based on an individual frame for the power levels indicated in the legend of the lower graphs. The gray crosses mark the results of measurements at other incident power levels. The lower graph indicates the associated distribution of received power. The noise floor level was measured by observing the received signal level above which the BER differed from 50%. For the case shown in Fig. 6, this value was -113.4 dBm.

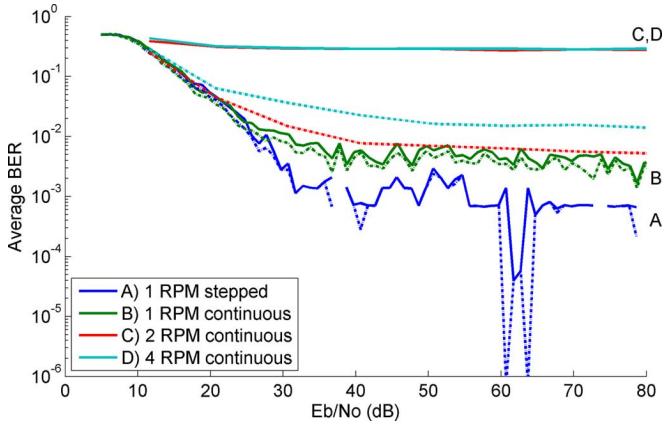

Fig. 7. Average BER versus Eb/No. Solid lines show the raw measurement, and dotted lines show the measurement with error correction applied.

We observed a strong occupation of two distinct BER levels. The high occupation of the lowest BER level corresponds to the occurrence of a single bit error per frame caused by the error-correcting algorithm. In our algorithm, a single bit error marks the position where the receiver has recovered from a loss of lock. The lowest level therefore marks the occurrence of a transition from a burst error that initially started in a previous frame. The burst error itself is marked by the second strongly occupied error level. This BER level occurs when only one small burst-error packet is created per frame.

These two distinct error levels are heavily occupied only because of the way our error-correcting algorithm recovers long-duration bit errors. They provide no information about the multipath channel, only about the receiver's inability to recover from a multipath event. In our analyses of the measurement results, these packets are filtered out so that the cause of the channel-induced bit errors can be studied. For the 24.3-ksps case shown, removing these fixed bit errors lowers the irreducible BER by approximately $1e-4$, increasing to 0.05 for lower received power values where more error correction is necessary due to the Gaussian receiver noise.

The need for the error-correcting algorithm is illustrated well in the plot in Fig. 7. The solid lines indicate the raw measurements, and the dotted lines indicate the results when the error-correcting algorithm was applied. The graph clearly shows that the error-correcting algorithm was especially necessary for the case of a 2- and a 4-rpm continuously moving paddle in order to find meaningful results in the propagation channel created by the reverberation chamber.

At lower received power (Eb/No) levels, the noise floor of the vector receiver is clearly apparent: When Gaussian noise dominates, there is an equal probability that a bit will be measured correctly or incorrectly for a BPSK signal, and the BER is 0.5. For higher values of received power, an irreducible BER is seen, corresponding to propagation channel effects created by the reverberation chamber. The goal of this work is to enable researchers to separate receiver effects from such reverberation-chamber-specific channel effects.

VII. Conclusion

To measure BER created by the reverberation chamber propagation environment, we discussed the issues related to use of laboratory instrumentation in the high-multipath, time-varying environment. The VSG sent an external trigger to the VSA as each frame was generated to attempt to synchronize the instruments. However, the reverberation chamber creates a different propagation-path length at each paddle position. We illustrated that the time-varying delay in the arrival of the first bit of a frame with respect to the external trigger may be determined by cross correlation of the ideal bit stream and the measured bits in post-processing pseudorandom sequence.

To reduce bias in the BER calculation as a result of the receiver's loss of symbol definition after a long fade, a simple error-correcting algorithm was developed for offline post-processing. The error-correcting algorithm allows study of the reverberation chamber BER effects, rather than BER arising from receiver-specific implementations. Practical implementation issues such as these can allow for study of the multipath channel created by the reverberation chamber itself, including the interaction of key wireless communications parameters such as the data rate, fade duration, and RMS delay spread, of which the latter can be controlled in the reverberation chamber using RF absorbing material.

Acknowledgment

The authors thank J. Ladbury and G. Koepke of NIST for their advice and technical support in this study, S. Prather of AT&T for helpful discussions, and A.G. Tijhuis of the Eindhoven University of Technology for advice and support.

References

[1] C. L. Holloway, D. A. Hill, J. M. Ladbury, P. F. Wilson, G. Koepke, and J. Coder, "On the use of reverberation chambers to simulate a Rician radio environment for the testing of wireless devices," *IEEE Trans. Antennas Propag.*, vol. 54, no. 11, pp. 3167–3177, Nov. 2006.

[2] N. Serafimov, P.-S. Kildal, and T. Bolin, "Comparison between radiation efficiencies of phone antennas and radiated power of mobile phones measured in anechoic chambers and reverberation chambers," in *Proc. IEEE AP-S Int. Symp.*, Jun. 2002, vol. 2, pp. 478–481.

[3] K. Rosengren and P.-S. Kildal, "Radiation efficiency, correlation, diversity gain, and capacity of a six monopole antenna array for a MIMO system: Theory, simulation and measurement in reverberation chamber," *Proc. Microw., Antennas Propag.*, vol. 152, no. 1, pp. 7–16, Feb. 2005.

[4] M. Lienard and P. Degauque, "Simulation of dual array multipath channels using mode-stirred reverberation chambers," *Electron. Lett.*, vol. 40, no. 10, pp. 578–5790, May 2004.

[5] K. Rosengren and P.-S. Kildal, "Study of distributions of modes and plane waves in reverberation chambers for characterization of antennas in multipath environment," *Microw. Opt. Technol. Lett.*, vol. 30, no. 20, pp. 386–391, Sep. 2001.

[6] M. Otterskog and K. Madsen, "On creating a nonisotropic propagation environment inside a scattered field chamber," *Microw. Opt. Technol. Lett.*, vol. 43, no. 3, pp. 192–195, Nov. 2004.

[7] C. Orlenius, P.-S. Kildal, and G. Poilasne, "Measurements of total isotropic sensitivity and average fading sensitivity of CDMA phones in reverberation chamber," in *Proc. IEEE AP-S Int. Symp.*, Washington, DC, Jul. 3–8, 2005, vol. 1A, pp. 409–412.

[8] M. Matsumoto and T. Nishimura, "Marsenne twister: A 623-dimensionally equidistributed uniform pseudo-random number generator," *ACM Trans. Model. Comput. Simul.*, vol. 8, pp. 3–30, Jan. 1998.

[9] E. Genender, C. L. Holloway, K. A. Remley, J. Ladbury, G. Koepke, and H. Garbe, "Use of reverberation chamber to simulate the power delay profile of a wireless environment," in *Proc. IEEE Int. Symp. EMC Eur.*, 2008, pp. 1–6.

[10] E. Genender, C. L. Holloway, K. A. Remley, J. Ladbury, G. Koepke, and H. Garbe, "Simulating the multipath channel with a reverberation chamber: Application to bit error rate measurements," *IEEE Trans. Electromagn. Compat.*, 2009, to be published.

[11] "Agilent vector signal analysis basics," Agilent, App. Note 150-15, 2004.